Cold-spraying coupled to nano-pulsed Nd-YaG laser surface pre-treatment

Christoulis, D. K.; Guetta, S.; Irissou, E.; Guipont, V.; Berger, M. H.; Jeandin, M.; Legoux, J.-G; Moreau, C.; Costil, S.; Boustie, M.; Ichikawa, Y.; Ogawa, K.

Publisher's version / Version de l'éditeur:
https://doi.org/10.1007/s11666-010-9500-5
Journal of Thermal Spray Technology, 19, 5, pp. 1062-1073, 2010-09-01

JTTEE5 19:1062–1073
DOI: 10.1007/s11666-010-9500-5
1059-9630/$19.00 © ASM International

Cold-Spraying Coupled to Nano-Pulsed Nd-YaG Laser Surface Pre-treatment

D.K. Christoulis, S. Guetta, E. Irissou, V. Guipont, M.H. Berger, M. Jeandin, J.-G. Legoux, C. Moreau, S. Costil, M. Boustie, Y. Ichikawa, and K. Ogawa

(Submitted December 22, 2009; in revised form February 25, 2010)

The effect of Al2017 substrate pre-treatment using pulsed laser ablation on adhesion strength of cold-sprayed Al coating is examined. A high energy pulsed laser beam was coupled with a cold-spray gun to result in laser ablation of the substrate surface a few milliseconds prior to the deposition. The influence of the laser fluence and repetition rate on substrate surface morphology and physico-chemical properties are investigated. Coating-substrate interfaces were observed using scanning electron microscopy (SEM) and transmission electron microscopy (TEM) of thin foils which were prepared using focused ion beam (FIB). Adhesion strength was evaluated by means of finite element method (FEM) of LAser Shock Adhesion Tests (LASAT). The results are compared to samples prepared on as received substrate, and pre-treated by two conventional methods, namely polishing and grit-blasting. It is shown that the coating-substrate interface is significantly improved when pulsed laser ablation is performed at optimized parameters. No oxide layer was found at the coating-substrate interface on laser ablated sample while two oxide layers were found on the as-received sample indicating that particle impingement transformed the native alumina layer in an amorphous Al oxide phase. The observations allow concluding that bonding of cold spray Al particles on Al2017 substrate requires either the removal of the native oxide layer or its transformation in an amorphous Al oxide phase.

Keywords adhesion, aluminum, bond strength, cold-spray, LASAT, pulsed laser ablation, substrate pre-treatment

1. Introduction

In thermal spray, coating adhesion strength is paramount since advanced coatings must remain bonded to the substrate under various and severe conditions. Many studies are devoted to the bonding mechanisms and to the optimization and improvement of coating bond strength in thermal spray (Ref 1-6). The same requirements of high coating adhesion hold true for cold spray coatings. However, the cold spray process differs from other thermal spray processes in its bonding mechanisms since there is no melting of the feedstock powder (Ref 7-13). Indeed, powder particles are accelerated in their solid state by a low temperature supersonic gas stream (Ref 14) and are plastically deformed upon impact on a substrate to form a coating. The particles can bond and form a coating only if they exhibit a material-dependant critical velocity (Ref 11-17). It has been shown that this critical velocity depends on surface conditions such as roughness and oxidation states (Ref 18-20), on particle state (Ref 21, 22) and on substrate material (Ref 23-25). It is often time concluded that the cold-sprayed particles adhere only on ''nascent'' surfaces (Ref 26) produced by the impacts of high-velocity sprayed particles which provoke the fracture of the pre-existing oxide layers of the substrate. However, the ''cleaning'' of substrate by sprayed particles can be characterized as an accidental method which induces the waste of the costly powders.

As for thermal spray, appropriate preparation of substrate surface prior to cold spraying contributes to the formation of high adhesive coatings. Coating's adhesion can be increased by means of conventional methods such as grit-blasting and chemical solvents (Ref 19-21). On the other hand, grit-blasting may provoke contamination of the substrate by grit inclusions, which in turns can decrease the fatigue resistance and induce thermal spray stresses while chemical solvents are hazardous and environmentally unfriendly.

The cleaning of the surface of the substrate by using pulsed laser ablation has already been successfully used for arc sprayed, plasma sprayed and HVOF coatings (Ref 27-36). High fluence laser pulses can remove both the contamination and oxide films at the surface thus enhancing coatings adhesion and limiting the recontamination of the deposited layers by condensed vapors. Coatings on laser ablation pre-treated substrates present

D.K. Christoulis, S. Guetta, V. Guipont, M.H. Berger, and **M. Jeandin**, Mines-ParisTech, C2P-Competence Center for Spray Processing, CNRS UMR 7633, Evry, France; **E. Irissou, J.-G. Legoux,** and **C. Moreau**, National Research Council Canada, Industrial Materials Institute, Montreal, QC, Canada; **S. Costil**, Université de Technologie de Belfort-Montbéliard, LERMPS, Belfort, France; **M. Boustie**, Laboratoire de Combustion et de Détonique, CNRS UPR 9028, ENSMA, Futuroscope, France; and **Y. Ichikawa** and **K. Ogawa**, Fracture & Reliability Research Institute, Tohoku University, Sendai, Japan. Contact e-mail: dimitris.christoulis@gmail.com.

higher bond strength compared to coatings formed on substrates pre-treated by conventional methods. Moreover, pulsed laser ablation process has further significant advantages compared to the classical pre-treatment methods: (i) it is a noiseless process and environmentally friendly, (ii) it has a high flexibility by using an improved laser delivery system, (iii) it can be easily monitored and automated.

In the present study, the effect of Al-alloy (AISI 2017) substrate pre-treatment and pulsed laser ablation on cold sprayed pure aluminum powder adhesion and coating build-up mechanisms is described. Optimized spray conditions were obtained based on particle velocity diagnostic and were used for the preparation of all samples. Prior to deposition, the substrates were either untreated (as-received), polished or grit blasted. Pulsed laser ablation, milliseconds prior deposition, was performed on untreated substrates under different laser conditions.

Coating-substrate interfaces were observed by scanning electron microscopy (SEM) and the percentage of interfacial cracks was calculated for every pre-treatment procedures and laser ablation conditions. SEM was also used to measure the mean thickness of the coatings as well as to observe substrate modifications which were induced by pulsed laser irradiation. Transmission electron microscopy (TEM) of thin foils, which were prepared using focused ion beam (FIB), was performed on selected samples to elucidate the main interaction mechanisms.

Coatings adhesion strength was evaluated by using LAser Shock Adhesion Testing, (LASAT) (Ref 37-46).

2. Materials and Processes

2.1 Cold-Spray and In-flight Velocity of the Al Particles

Fine aluminum powder (Alfa Aesar, MA, 17-35 μm) of spherical morphology was sprayed using a KINETICS® 3000-M System (CGT-GmbH, Ampfing, Germany). A polymeric nozzle (PBI-33, CGT-GmbH) was supplied for the spraying of Al-based materials which prevents from nozzle clogging. The nozzle PBI-33 has round exit of 10 mm diameter, expansion ratio of 13.7, divergent section length of 178 mm, throat diameter of 2.7 mm and total length of 220 mm.

The spraying experiments were carried out by using nitrogen (N_2) as the propelling gas. Maximum particle velocity is obtained at the maximum inlet gas temperature and pressure. The inlet gas temperature was then set to 350 °C, which is the upper limit to avoid any degradation of the nozzle material, while inlet gas pressure was set to 3.0 MPa which is the maximum stable operating condition of KINETICS® 3000-M System.

The ColdSprayMeter® (Tecnar Automation Inc., St-Bruno, QC, Canada) was used in order to measure the particle's mean velocity for various standoff distances. The standoff distance of 20 mm was chosen as the most appropriate one. For this distance the mean velocity of the aluminum cold-sprayed particles was measured to be 792 $m \cdot s^{-1}$ significantly higher than the reported critical velocity for pure aluminum on aluminum substrate (Ref 13, 22).

2.2 Pre-treatment of Substrate

AISI 2017 substrates were used either wrought (as-received), grit-blasted with 300 μm angular alumina particles or polished to 1 μm diamond powder. All the substrates were cleaned in an ultrasonic bath and prior to the cold spraying the substrates were cleaned by using alcohol and compressed air.

As-received substrates were laser ablated using the PROTAL® (Quantel, Lannion, France), a commercial laser ablation equipment designed for surface preparation of substrates for thermal spraying. PROTAL® is equipped with two Q-switched Nd-YAG lasers operating at $\lambda = 1.064$ μm with an average power output of 40 W each (270 mJ per pulse with adjustable frequency up to 150 Hz) and with a pulse duration (FWHM) of approximately 10 ns. The laser beam has a rectangular shape with a ''top-hat'' energy distribution thanks to a specific optical arrangement (Ref 30).

Table 1 summarizes the diverse pre-treatment and laser ablation conditions used for this study.

Considering the gun traverse speed, the laser frequencies, and the laser spot sizes (Fig. 1d), an arithmetic exercise suffices to calculate the overlapping percentage for each set of conditions (Table 1).

The laser head of PROTAL® was coupled with the cold-spray gun to result in the laser beam passing milliseconds prior to the cold-spray jet for deposition (Fig. 1). For that, the scanning of the substrate was realized in a specific way (Fig. 1c). The same movement geometry was chosen also for the conventionally prepared substrates since experiments indicate that substrate temperature increases during spraying due to the heated propelling gas (Ref 43). Hence, a unique movement geometry (Fig. 1c) was chosen to introduce uniform heat input to the substrate for all the spraying experiments.

Pulsed Nd-YAG lasers were operated only during the first pass in order to clean the substrate surface. The surface preparations and sprayings experiments were carried out in the MAMADC cold-spray laboratory located at the Industrial Materials Institute of the National Research Council of Canada.

Table 1 Pre-treatment of substrates

Substrate	Laser energy density, $J \cdot cm^{-2}$	Frequency, Hz	Overlapping of two pulses, %
As-received	No laser	No laser	No laser
Polished	No laser	No laser	No laser
Grit-blasted	No laser	No laser	No laser
As-received	1.0	37.5	24
As-received	1.0	150	82
As-received	2.2	18.75	No overlapping
As-received	2.2	37.5	47
As-received	2.2	150	87

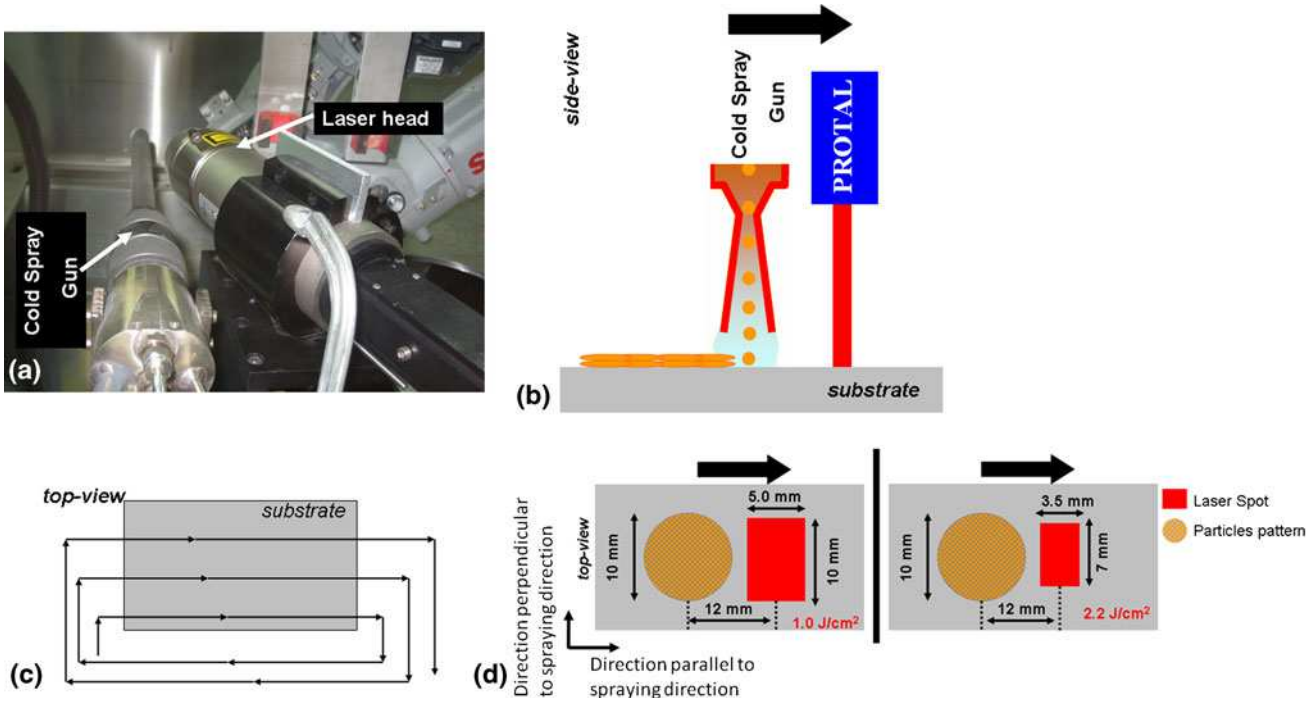

Fig. 1 (a) Experimental set-up, (b) side view of experimental set-up, (c) movement geometry of coupled cold-spray gun-laser head and (d) top view of the pattern of both cold-sprayed particles and laser spot

2.3 Coating Characterization

SEM (LEO 450VP, Germany) was used to investigate the microstructure of the coatings and the interfaces between substrate and coatings. For the SEM images standard conditions were chosen: working distance of 13 mm and voltage of 15 kV in backscatter mode. The percentage of cracked interfaces was determined by means of quantitative image analysis (ImageJ®; Ref 44). About 10 mm of interface was examined in direction parallel and perpendicular to the spraying direction (Fig 1d). The examined 10 mm correspond to about 60 SEM images of high magnification (×1000) for each direction. The mean thickness of the cold-sprayed coatings was also quantitatively calculated via image analysis of SEM images.

Thin foils of coating-substrate interface of selected specimens were prepared by FIB for observation by transmission electron microscopy using a 200 kV FEG-TEM-STEM equipped with an energy-dispersive x-ray spectrometer (FEI Tecnai F20 and EDAX, The Netherlands).

2.4 Laser Shock Adhesion Test (LASAT)

LASAT was used to measure the adhesion of the coatings and has been described in detail in previous articles (Ref 37-46). Basically, LASAT consists in irradiating the rear surface of a substrate with a laser to generate a shock wave. This shock wave propagates and reflects in the material into a release wave crossing the unloading wave leading to tensile stresses.

LASATestings were carried out by using a Nd:YAG laser delivering 25 ns Gaussian pulses (LCD, ENSMA, Poitiers, France). The laser was focused on a 4-mm diameter spot through a water confinement at the rear surface of the substrate with a wide range of laser power densities (1.7-4.3 GW · cm^{-2}).

During the LASATesting, Doppler laser interferometry using a Velocity Interferometer System for Any Reflector (VISAR) was applied to the coating surface to measure its velocity as a function of time.

2.5 Numerical Simulation of Bond Strength

For the determination of the level of traction generated in the coating during LASAT, simulation of the propagation of the applied shock into the target (substrate) is required (Ref 40). 2D numerical simulations were developed using the Explicit version of the finite element code Abaqus® (Ref 41). Thus, 2D wave propagation mechanisms (Ref 41, 42) were taken into account to calculate the tensile traction at the interface. The numerical simulation of bond strength of coatings by using FE method has been described in detail in previous articles (Ref 39-42).

Using jointly experiments and 1D numerical simulation (Ref 42), the pressure intensity applied to the rear surface of the coating was previously estimated as a function of the laser power density. In an axisymmetric configuration, numerical sensors were set on the laser axis, from the coating-substrate interface to the coating free surface, where the VISAR measurement was experimentally carried out. To take into account the assumed isothermal

dynamic behavior under shock, materials were modeled with a simplified Johnson-Cook constitutive law (Ref 45).

$$\sigma = \left(A + B \cdot \varepsilon_p^n\right) \cdot \left(1 + C \cdot \ln\left(\frac{\dot{\varepsilon}}{\dot{\varepsilon}_0}\right)\right) \quad \text{(Eq 1)}$$

where A is the yield stress, B and n represent the effect of strain hardening, ε_p the equivalent plastic strain and $\dot{\varepsilon}/\dot{\varepsilon}_0$ the dimensionless plastic strain rate for $\dot{\varepsilon}_0 = 10^6\ S^{-1}$.

The four parameters of the Johnson-Cook Law (Eq 1) of the materials that were examined are listed in Table 2.

3. Results

3.1 Laser Irradiation Effects

Cracks and traces, which should have been induced during the production of the hot rolled Al alloy material, were found on the surface of the as-received substrates (Fig. 2).

The observations of the ablated substrate revealed that for low energy density ($1.0\ J \cdot cm^{-2}$), the pulsed laser beam reacted only with the cracks provoking slight fusion at their borders (white arrows, Fig. 3a). Also, craters were formed after laser irradiation (white circles, Fig. 3a). These craters are correlated either with the surface defects such as micro-inclusions and small scratches present prior to irradiation or with the existence of precipitated phases (Al_2Cu) of the used AISI 2017 alloy (Ref 48).

The increase of laser energy density to $2.2\ J \cdot cm^{-2}$ resulted in a strong change in surface morphology (Fig. 3b, c). Extensive substrate melting is observed. The pre-existing cracks disappeared and few craters (white circles, Fig. 3b) are still visible. Substrate surface seems to smoothen with the increase in the laser frequency (Fig. 3c), probably as a result of re-melting which is provoked by the high overlapping phenomenon.

Table 2 Numerical parameters used for simulation (Ref 45-47)

	A, MPa	*B*, MPa	*C*	*n*
Aluminum powder	130	160	0.014	0.36
AISI 2017 substrate	265	426	0.015	0.34

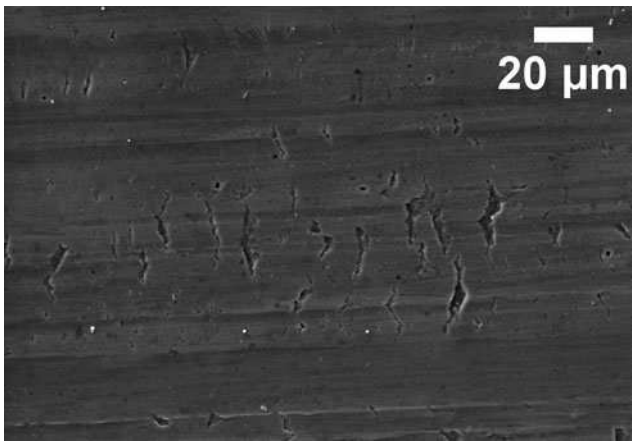

Fig. 2 SEM top view of as-received substrate

3.2 Single Pass of Cold-Sprayed Al

First, the gun and the laser head PROTAL® carried out a single pass onto an as-received AISI 2017 substrate.

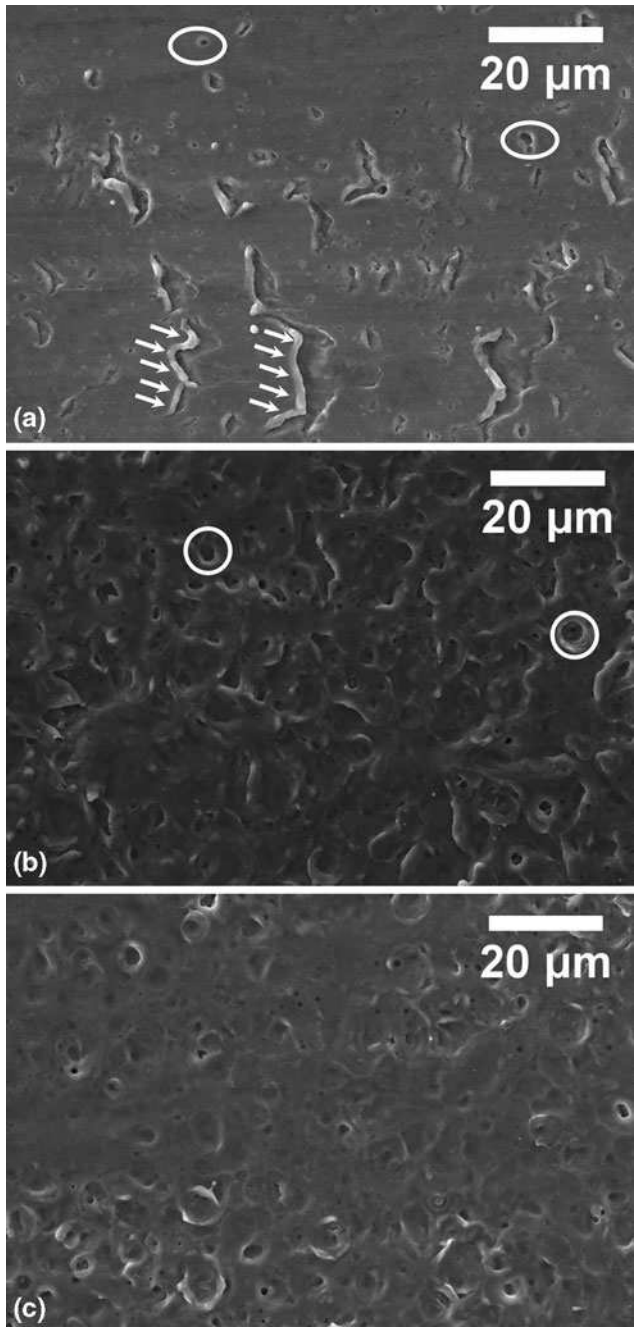

Fig. 3 SEM top view of substrate surfaces after laser irradiation: (a) $1.0\ J \cdot cm^{-2}$, 150 Hz, (b) $2.2\ J \cdot cm^{-2}$, 37.5 Hz, (c) $2.2\ J \cdot cm^{-2}$, 150 Hz

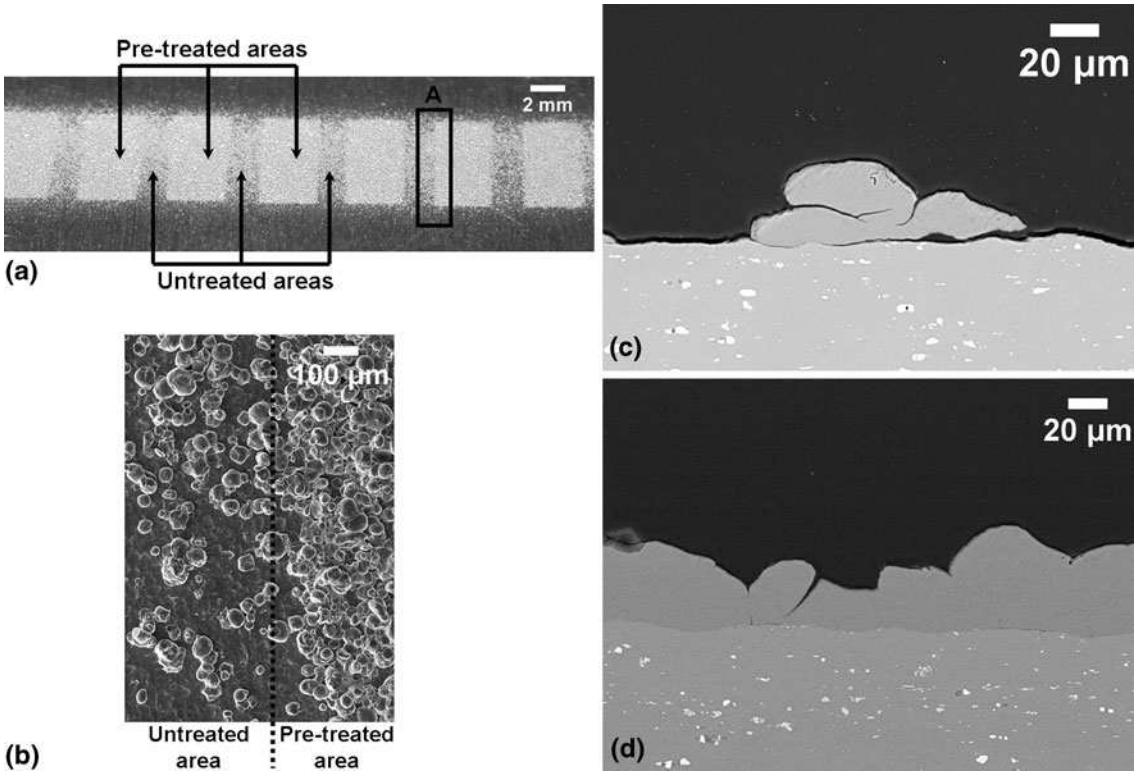

Fig. 4 (a) Macroscopic photo of the untreated and pre-treated areas, (b) magnification of area "A" (SEM image), (c) SEM cross section of the untreated area, (d) SEM cross section of the pre-treated (2.2 J · cm^{-2}, 18.75 Hz)

For this case, the maximum laser energy (2.2 J · cm^{-2}) was selected while the laser frequency was set to 18.75 Hz. Under this low laser frequency, no overlapping of laser pulses took place (Table 1) and thus two distinguished areas were created: untreated and laser ablated areas.

It was observed that on the untreated areas only few particles remained adhering (Fig. 4). Furthermore, the SEM observations of the cross-section of the untreated areas revealed that these particles have weak adhesion with the substrate (Fig. 4c).

On the other hand, the number of the deposited particles adhered to the laser ablated areas was strongly increased and a coating was formed on the AISI 2017 substrate (Fig. 4d). In addition, the adhesion of the coating onto the laser ablated areas seems better (Fig. 4d) than that of the untreated sample (Fig. 4c), as significantly less gap is observed between the coating and the substrate.

3.3 Formation of Thick Aluminum Coatings

For the formation of thick aluminum coatings, laser frequencies (37.5 Hz and 150 Hz, Table 1) were selected to insure laser irradiation over the whole surface of the substrate.

3.3.1 Coatings Thickness. Thick coatings were deposited on the substrates (see Fig. 5). Coating mean thicknesses were almost the same for conventionally prepared substrates and for low energy (1.0 J · cm^{-2}) irradiated substrates (Table 3).

Significant increase (≈80-90 µm) of the mean thickness was observed with the increase of laser energy density from 1.0 to 2.2 J · cm^{-2}. Interestingly, the difference in coating thickness of coatings deposited on untreated and on laser ablated (2.2 J · cm^{-2}, 37.5 Hz) substrate is around 50 µm. One can conclude that this difference corresponds well to the difference of average coating thickness as shown in Fig. 4. The improved deposition efficiency with high fluence laser ablation is due essentially to the adhesion of a higher fraction of particles during the first pass as compared to other surface pre-treatment and laser ablation conditions. Nevertheless, it is clear that a large fraction of the impinging particles are not deposited during the first pass even at higher laser ablation fluence and so they should contribute to the surface modification as well.

3.3.2 Coating-Substrate Interface. Representative interfaces between thick coating and the substrate are presented in Fig. 6. It was found that grit-blasting and polishing pre-treatment did not offer any reduction of cracks observed on the as-received substrates (Table 4). Surprisingly, grit-blasting of the substrate contributed to the increase of the percentage of cracked interface (Table 4). Also in the case of grit-blasted substrates, the alumina particles entrapped onto the substrate were seen (Fig. 6b).

Conversely, laser ablation with PROTAL® promoted a better interface with much less interfacial cracks (Table 4). For the highest laser energy density (2.2 J · cm^{-2}) and under the highest frequency (150 Hz), cracks could

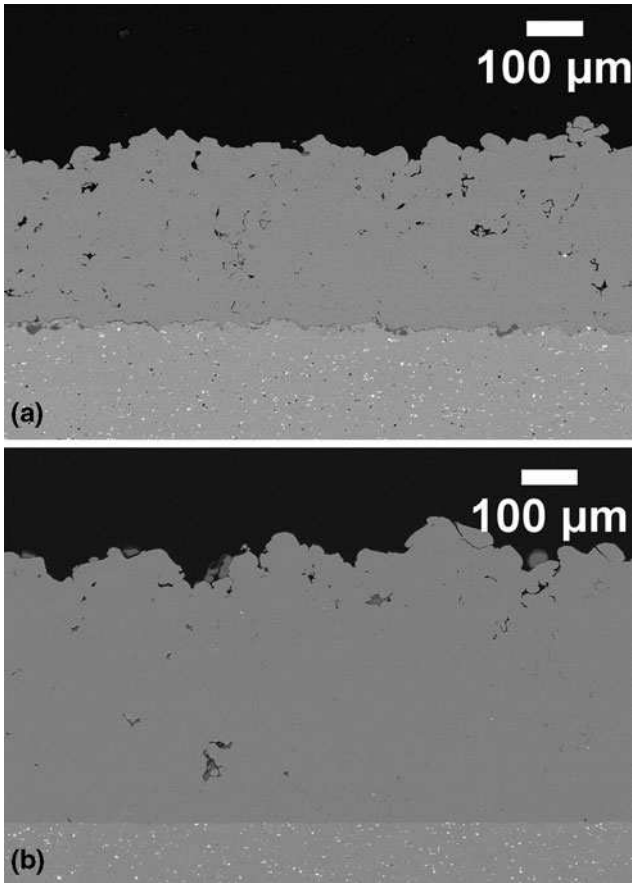

Fig. 5 SEM of cross-sections of cold-sprayed Al coatings formed onto (a) grit-blasted substrate, (b) laser irradiated substrate (2.2 J · cm^{-2}, 150 Hz)

Table 3 Mean thickness of the coatings

Substrate	Laser energy density, J · cm^{-2}	Frequency, Hz	Mean thickness, µm
As-received	No laser	No laser	340 ± 17
Polished	No laser	No laser	305 ± 19
Grit-blasted	No laser	No laser	324 ± 6
As-received	1.0	37.5	310 ± 9
As-received	1.0	150	323 ± 16
As-received	2.2	37.5	393 ± 10
As-received	2.2	150	410 ± 13

barely be found in direction perpendicular to spraying and did not appear at all in the parallel direction (Fig. 6c).

The difference of the percentage of interfacial cracks between parallel and perpendicular is due to the difference in the size of the particle jet compared to the size of the laser spot (Fig. 1). In the perpendicular direction, fraction of sprayed particles impact on untreated areas and so these particles can present weaker adhesion as shown in Fig. 4(a) and (c). On the other hand, in the parallel direction, cold-sprayed particles always impact on laser pre-treated areas, if the cross-section metallographic

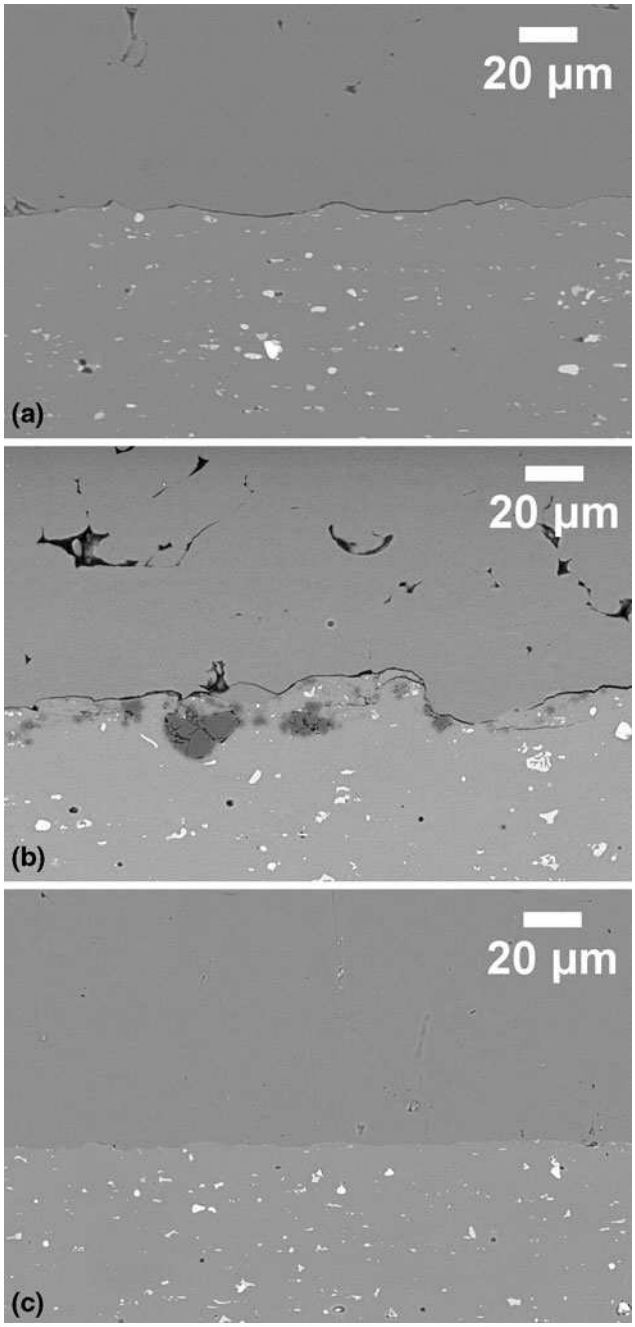

Fig. 6 SEM of cross-sections of cold-sprayed Al coatings formed onto (a) as-received substrate, (b) grit-blasted substrate, (c) laser irradiated substrate (2.2 J · cm^{-2}, 150 Hz)

sample is prepared properly, and thus along this direction a reduced percentage of interfacial cracks is observed.

3.3.3 TEM Observations. Thin foils of Al-coatings were prepared by FIB and examined with TEM (Fig. 7 and 8).

A typical oxide layer of about 100 nm in thickness could be observed at the coating-substrate interface in cold-sprayed ''as-received'' Al 2017. The EDX indicate that this oxide layer is in fact divided into two regions of

distinct Al/O ratio (in gray in Fig. 7a) The layer at the substrate side has the stoichiometry of alumina, indicating that it is the native oxide while the other one at the coating side is richer in oxygen (~35 wt.% Al, 65 wt.% O).

TEM analysis indicates that the oxide layer at the coating side is amorphous since the grey contrast of this oxide layer was constant. Furthermore, EFTEM (Energy Filtered Transmission Electron Microscope) with GIF (Gatan Image Filter) image recorded on the low loss region (Plasmon) of the EELS spectrum highlights this interfacial layer, which is characteristic of amorphous structure (Ref 49).

Table 4 Percentage of interfacial cracks in direction parallel (//) and perpendicular (⊥) to spraying direction

Substrate	Laser energy density (J · cm^{-2})	Frequency (Hz)	% Cracks //	% Cracks ⊥
As-received	No laser	No laser	22	23
Polished	No laser	No laser	21	21
Grit-blasted	No laser	No laser	29	27
As-received	1.0	37.5	15	19
As-received	1.0	150	14	17
As-received	2.2	37.5	11	13
As-received	2.2	150	0	4

The transformation of the native alumina oxide to an amorphous Al oxide could be the result of extensive peening by the impinging particles (similar to what is observed in mechanical milling for example; Ref 50, 51). Indeed, it was reported that amorphization can occur during cold spraying (Ref 52). It is interesting to note that most of the cracks observed at the interface were propagated in-between the two oxides.

In contrast, for laser-processed Al 2017, no oxygen could be detected at the interface (Fig. 8) neither on STEM images nor by EDX profile. This profile was obtained with a probe size of 1 nm (enlarged to 3 nm at the exit side of the thin foil), 10 nm between the consecutive analysis spots, and a limit of detection of 1 wt.% for O. It can therefore be inferred that the native layer was removed by the laser treatment, and if an oxide thinner layer was formed prior to the particle reached the substrate, the thickness of this layer would not exceed a few nanometers.

Furthermore, the oxide layer of the particles normally has been destroyed due to the high-particle velocity (Ref 53, 54). In order to crash the oxide layer of the particles, the particles should have velocity higher than the

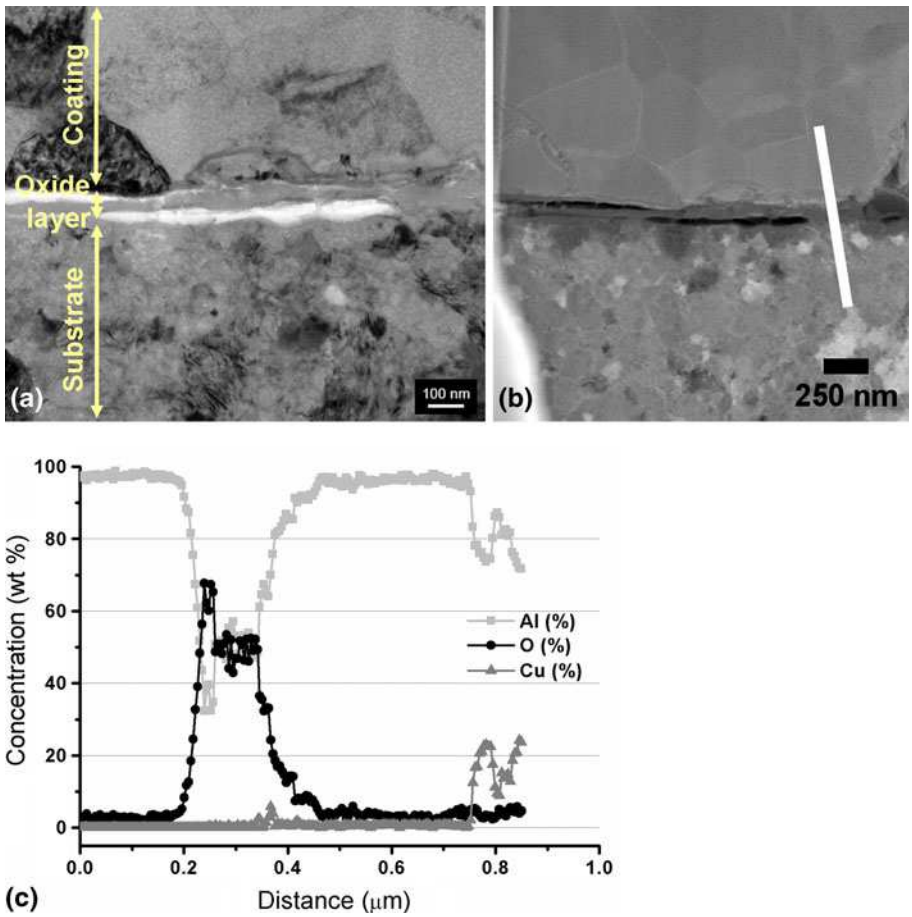

Fig. 7 TEM pictures of cold-sprayed Al on as-received AISI 2017 substrate (a) Bright Field (BF) image, (b) HAADF (High Angle Annular Dark Field) image, (c) EDX profiles along the white line

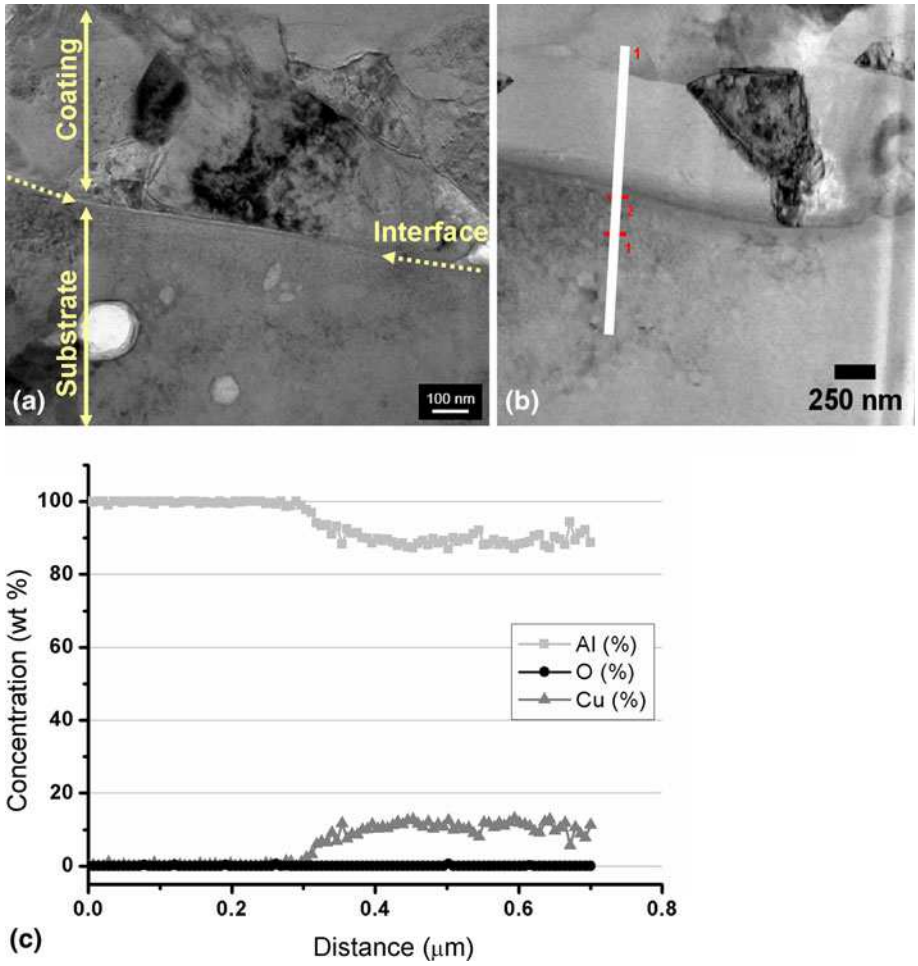

Fig. 8 TEM pictures of cold-sprayed Al on laser pre-treated (2.2 J · cm^{-2}, 150 Hz) AISI 2017 substrate: (a) Bright Field (BF) image, (b) HAADF (High Angle Annular Dark Field) image, (c) EDX profiles along the white line

critical velocity (Ref 53, 54). ColdSprayMeter was used in order to ensure that the velocity of Al-particles is significantly higher than the reported critical velocity for pure aluminum on aluminum substrate (Ref 13, 22). These crushed oxide films can be removed by the formation of jetting at the local deformed zones (Ref 55-57).

3.4 LASATesting

Laser shock adhesion testing was performed both on coating formed onto as-received substrates and onto laser irradiated substrates (2.2 J · cm^{-2}, 150 Hz).

The lower adhesion of Al-coatings onto as-received substrates was confirmed by LASAT experiments. Coatings were totally de-bonded with the lower laser energy (1.7 GW · cm^{-2}) (Fig. 9a). These results are confirmed also by VISAR signals (see Fig. 10). The velocity peaks corresponded to shock wave interaction with the coating surface. For both LASAT energies, the absence of negative peaks corresponds to the damage of coating-substrate interface (Ref 38).

Onto pre-treated substrates (2.2 J · cm^{-2}, 150 Hz), cold-sprayed aluminum coatings presented higher adhesion. When low laser energy (1.7 GW · cm^{-2}, Fig. 9b) was used, the coating remained adherent. The increase of LASAT energy (2.6 GW · cm^{-2}, Fig. 9c) provoked the interlamelar cracking of the Al-coatings. This revealed that the cohesion of the coatings (bonding of cold-sprayed Al-Al) was weaker compared to the coating-substrate adhesion. Similar phenomenon has been found for cold-sprayed copper on AISI 2017 substrate (Ref 38).

At higher LASAT laser energy (4.3 GW · cm^{-2}), the coating was de-bonded from the laser pre-treated substrate (Fig. 9c). However, few particles still remained bonded reveling the high achieved adhesion strength.

For laser pre-treated substrates the VISAR results are well segregated (Fig. 10). For low LASAT energy (2.6 GW · cm^{-2}, black line), the aluminum surface velocity showed negative values after the first positive peak. The positive velocity peaks correspond to shock wave interaction with the coating surface while the negative peaks correspond to tensile stresses reaching the substrate surface (Ref 38). The tensile stresses were those generated at

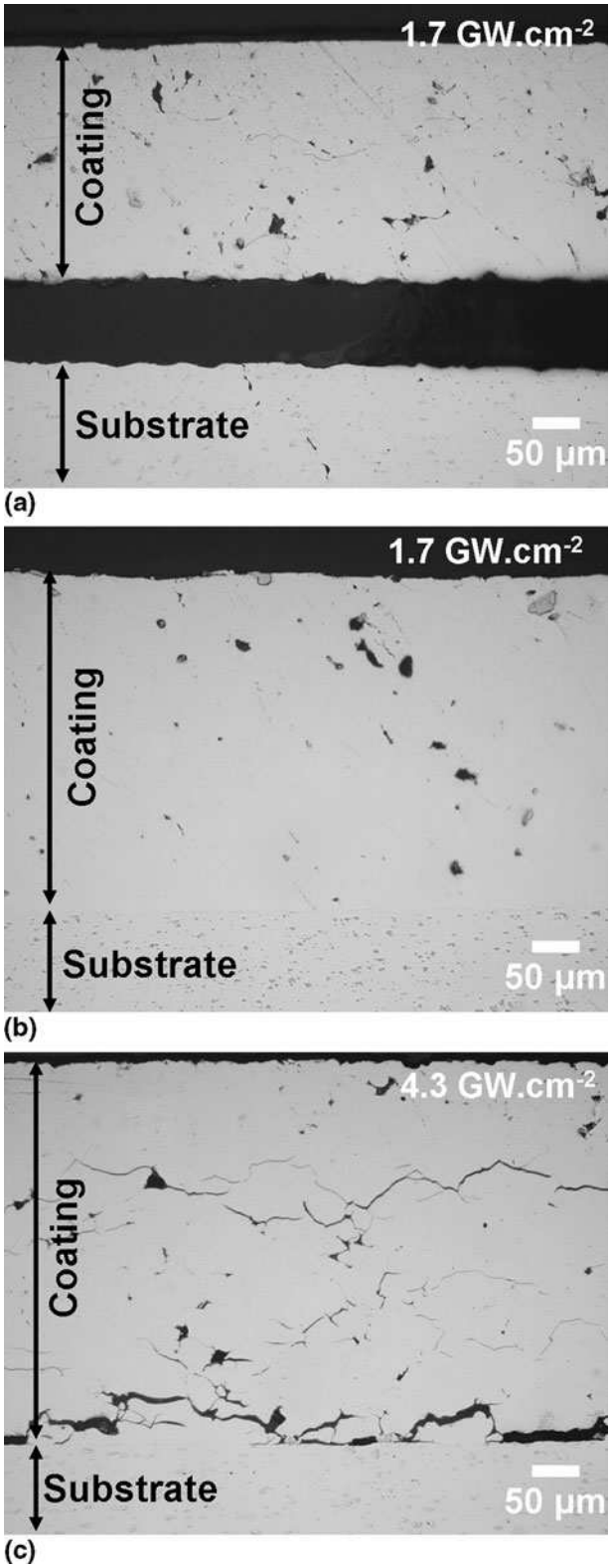

Fig. 9 Cross-section optical image of LASATested interface of cold-sprayed Al onto (a) as-received substrate when the applied LASAT energy was 1.7 GW · cm^{-2}; (b) laser pre-treated (PROTAL 2.2 J · cm^{-2}, 150 Hz) substrate when the applied LASAT energy was 1.7 GW · cm^{-2}; (c) laser pre-treated (PROTAL 2.2 J · cm^{-2}, 150 Hz) substrate when the applied LASAT energy was 4.7 GW · cm^{-2}

the aluminum surface, after their propagation through the whole sample. On the other hand, for high LASAT energy (4.6 GW · cm^{-2}), only a positive peak was detected since the tensile wave reflected on the thus-created cracks and the surface coating velocity did not show negative values. The tensile stress at the interface, σ22, was calculated from modeling/numerical simulation of 1D and 2D shock wave effects within the coating-substrate system and averaged over the whole laser spot (Ref 39). Bonding strength value could therefore be determined from ''post-mortem'' observation of interfacial cross-sections and study of VISAR velocity profiles (Fig. 10) during the test since both show when the coating de-bonds (Fig. 10). The bond strength was found to be above 629 MPa but below 681 MPa for laser-ablated Al 2017 compared to below (one may assume much below) 562 MPa for as-received Al 2017. These bond strength values are significantly higher than what is typically reported for pull-off ASTM C633 testing which lies in the 10-80 MPa range (Ref 19-25, 58-61), while for some conditions of aluminum coating applied on aluminum 7075 alloy substrate the failure mode was in the glue at over 60 MPa (Ref 62).

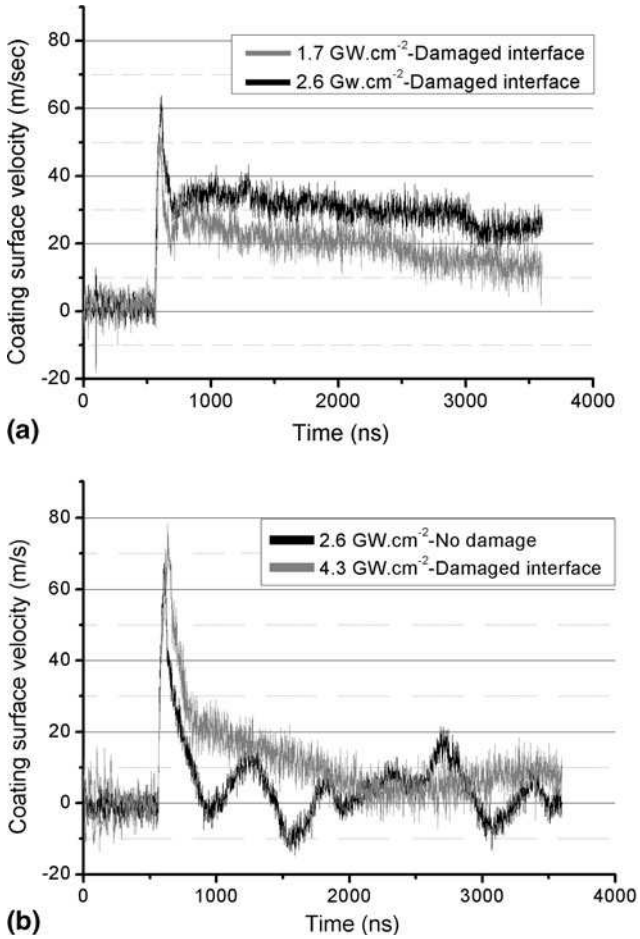

Fig. 10 Velocity profiles of cold-sprayed Al surface on (a) as-received AISI 2017 substrate; (b) laser pre-treated (2.2 J · cm^{-2}, 150 Hz) substrate AISI 2017

The difference between the adhesion levels measured using a dynamic (laser shock) test and a conventional (''pull-off'') static test is expected due to the difference in loading duration. Arrigoni et al. (Ref 63) have measured the adhesion of plasma-sprayed copper on aluminum substrate by using the LASATesting as well as other conventional techniques (EN 582, similar to ASTM C633, and bulge and blister test) and a difference on the adhesion values was found. These experiments have evidenced the ability of LASAT to discriminate various adhesion levels. For a given threshold, the energy to debond the materials estimated according to each technique was similar, though the amplitude of the tensile stress was much higher with laser shocks. As the duration during which the traction is applied is of the order of a few tens of ns, the bulk materials strength is much higher than the quasi-static strength of materials. Therefore, with a laser shock of a few ns, the aluminum strength is higher than 1.6 GPa (Ref 64, 65). When LASAtesting a substrate-coating assembly, usually the interface is the weakest point and considering the increase of the materials strength under such extreme strain rate loadings, usually the interface will be the first point to break with no damaging of the other materials. As in the case of bulk materials damaging, the debonding tensile strength of interfaces delivered by the LASATest is much higher than the one provided by more conventional (less dynamic) techniques, but the energy locally absorbed by the material is very similar (Ref 63).

4. Conclusions

This study focused on the effect of pulsed laser ablation pre-treatment on the adhesion of cold-sprayed aluminum coating onto AINSI aluminium alloy substrate. The main conclusions are summarized as follows:

- Cross section micrographs revealed that in the range of 21-29% of the interface length are cracked on samples prepared with grit blasted, polished or wrough substrates. On the contrary, no interfacial crack could be seen on the sample prepared with the optimized laser ablation conditions (2.2 J · cm^{-2}, 150 Hz, PROTAL®).
- At optimized laser ablation conditions, a continuous layer is deposited during the first pass while on other substrate preparations a continuous coating is obtained during the second pass. Higher thickness is thus obtained on laser ablation prepared substrate as compared to other substrate pre-treatment.
- On as received substrate the coating build up process resulted in transformation in the crystalline structure of the native oxide layer. TEM revealed that an amorphous aluminium oxide phase was created at the interface on the coating side while an alumina layer is still present on the substrate side.
- Most of the cracks observed at the interface were propagated in between the two oxides. The adhesive strength between the aluminium coating and the amorphous aluminium oxide layer thus seems higher than that between the two oxide layers.
- Pulsed laser ablation at optimized conditions eliminated the native oxide at the substrate surface.
- The bond strength of Al cold-sprayed coating was numerically calculated from LASAT measurements and it was found to lie in between 629 and 681 MPa for samples prepared on laser pre-treated substrates (2.2 J · cm^{-2}, 150 Hz) and below 562 MPa on as-received substrate.
- Laser ablation energy density and repetition rate must be optimized to insure melting of the substrate surface for optimal effect on adhesive strength.

Acknowledgments

The authors would like to thank Mr. B. Harvey and Mr. M. Lamontagne both of Industrial Material Institute (Boucherville, Canada) for Cold-spray and PROTAL® process, respectively. Mr. K. Sagakuchi and Dr. T. Miyazaki, both of Tohoku University (Sendai, Japan) are acknowledged for FIB cuttings. The current project was carried out in the framework of the Cold-spray Club (www.mat.ensmp.fr/clubcoldspray).

References

1. J. Day, X. Huang, and N.L. Richards, Examination of a Grit-Blasting Process for Thermal Spraying Using Statistical Methods, *J. Therm. Spray Technol.*, 2005, **14**(4), p 471-479
2. P. Araujo, D. Chicot, M. Staia, and J. Lesage, Residual Stresses and Adhesion of Thermal Spray Coatings, *Surf. Eng.*, 2005, **21**(1), p 35-40
3. O.C. Brandt, Mechanical Properties of HVOF Coatings, *J. Therm. Spray Technol.*, 1995, **4**(2), p 147-152
4. D.J. Greving, J.R. Shadley, E.F. Rybicki, D.J. Greving, J.R. Shadley, and E.F. Rybicki, Effects of Coating Thickness and Residual Stresses on the Bond Strength of ASTM C633-79 Thermal Spray Coating Test Specimens, *J. Therm. Spray Technol.*, 1994, **3**(4), p 371-378
5. S.P. Lu and O.Y. Kwon, Microstructure and Bonding Strength of WC Reinforced Ni-Base Alloy Brazed Composite Coating, *Surf. Coat. Technol.*, 2002, **153**(1), p 40-48
6. M.F. Bahbou, P. Nylen, and J. Wigren, Effect of Grit Blasting and Spraying Angle on the Adhesion Strength of a Plasma-Sprayed Coating, *J. Therm. Spray Technol.*, 2004, **6**(2), p 508-514
7. H. Assadi, F. Gartner, T. Stoltenhoff, and H. Kreye, Bonding Mechanism in Cold Gas Spraying, *Acta Mater.*, 2003, **51**, p 4379-4394
8. R.C. Dykhuizen, M.F. Smith, D.L. Gilmore, R.A. Neiser, X. Jiang, and S. Sampath, Impact of High Velocity Cold Spray Particles, *J. Therm. Spray Technol.*, 1999, **8**(4), p 559-564
9. S. Guetta, M.H. Berger, F. Borit, V. Guipont, M. Jeandin, M. Boustie, Y. Ichikawa, K. Sakaguchi, and K. Ogawa, Influence of Particle Velocity on Adhesion of Cold-Sprayed Splats, *J. Therm. Spray Technol.*, 2009, **18**(3), p 331-342
10. T. Hussain, D.G. McCartney, P.H. Shipway, and D. Zhang, Bonding Mechanisms in Cold Spraying: The Contributions of Metallurgical and Mechanical Components, *J. Therm. Spray Technol.*, 2009, **18**(3), p 364-379
11. D.L. Gilmore, R.C. Dykhuizen, R.A. Neiser, T.J. Roemer, and M.F. Smith, Particle Velocity and Deposition Efficiency in the

Cold Spray Process, *J. Therm. Spray Technol.*, 1999, **8**(4), p 576-582
12. T. Stoltenhoff, H. Kreye, and H.J. Richter, An analysis of the Cold Spray Process and Its Coatings, *J. Therm. Spray Technol.*, 2002, **11**(4), p 542-550
13. T. Schmidt, F. Gärtner, H. Assadi, and H. Kreye, Development of a Generalized Parameter Window for Cold Spray Deposition, *Acta Mater.*, 2006, **54**(3), p 729-742
14. E. Irissou, J.G. Legoux, A.N. Ryabinin, B. Jodoin, and C. Moreau, Review on Cold Spray Process and Technology: Part I—Intellectual Property, *J. Therm. Spray Technol.*, 2008, **17**(4), p 495-516
15. A. Papyrin, V. Kosarev, and S. Klinkov, *Cold Spray Technology*, Elsevier, Oxford, 2007, p 328
16. V.K. Champagne, *The Cold Spray Materials Deposition Process: Fundamentals and Applications*, Woodhead Publishing, Cambridge, 2007, p 362
17. R.G. Maev and V. Leshchynsky, *Introduction to Low Pressure Gas Dynamic Spray: Physics & Technology*, Weinheim 2008: Wiley-VCH. 234p
18. L. Ajdelsztajn, A. Zuniga, B. Jodoin, and E.J. Lavernia, Cold Gas Dynamic Spraying of a High Temperature Al Alloy, *Surf. Coat. Technol.*, 2006, **201**, p 2109-2211
19. S. Kumar, G. Bae, and C. Lee, Deposition Characteristics of Copper Particles on Roughened Substrates Through Kinetic Spraying, *Appl. Surf. Sci.*, 2009, **255**(6), p 3472-3479
20. B.T. Golesich and K. Anderson, Effects of Surface Preparation on the Performance of Cold Spray Coatings, *Proceeding of 19th AeroMat Conference & Exposition*, 23-26 June 2008, Austin, TX, USA
21. S. Kumar, G. Bae, K. Kang, S. Yoon, and C. Lee, Effect of Powder State on the Deposition Behaviour and Coating Development in Kinetic Spray Process, *J. Phys. D. Appl. Phys.*, 2009, **42**(7), p 1-8
22. E. Irissou, J.G. Legoux, B. Arsenault, and C. Moreau, Investigation of Al-Al_2O_3 Cold Spray Coating Formation and Properties, *J. Therm. Spray Technol.*, 2007, **16**(5-6), p 661-668
23. J. Wu, J. Yang, H. Fang, S. Yoon, and C. Lee, The Bond Strength of Al-Si Coating on Mild Steel by Kinetic Spraying Deposition, *Appl. Surf. Sci.*, 2006, **252**(22), p 7809-7814
24. D. Zhang, P.H. Shipway, and D.G. McCartney, Cold Gas Dynamic Spraying of Aluminum: The Role of Substrate Characteristics in Deposit Formation, *J. Therm. Spray Technol.*, 2005, **14**(1), p 109-116
25. T. Marrocco, D.G. McCartney, P.H. Shipway, and A.J. Sturgeon, Production of Titanium Deposits by Cold-Gas Dynamic Spray: Numerical Modeling and Experimental Characterization, *J. Therm. Spray Technol.*, 2006, **15**(2), p 263-272
26. Y. Ichikawa, T. Miyazaki, K. Ogawa, T. Shoji, and M. Jeandin, Deposition Mechanism of Cold Sprayed MCrAlY Coatings Focused on Nanostructure, *Thermal Spray 2008: Thermal Spray Crossing Borders*, on CD-ROM, E. Lugscheider, Ed., June 2-4, 2008 (Maastricht, The Netherlands), DVS Deutscher Verband für Schweißen, 2008, p 283-287
27. S. Barradas, M. Jeandin, C. Bolis, L. Berthe, M. Arrigoni, M. Boustie, and G. Barbezat, Study of Adhesion of PROTAL® Copper Coating of Al 2017 Using the Laser Shock Adhesion Test (LASAT), *J. Mater. Sci.*, 2004, **39**, p 2707-2716
28. H. Li, S. Costil, H.-L. Liao, and C. Coddet, Role of the Laser Surface Preparation on the Adhesion of Ni-5%Al Coatings Deposited Using the PROTAL Process, *J. Therm. Spray Technol.*, 2006, **15**(2), p 191-197
29. H. Li, S. Costil, S.-H. Deng, H-L. Liao, C. Coddet, V. Ji, and W-J. Huang, Benefit of Surface Oxide Removal on Thermal Spray Coating Adhesion Using the PROTAL process, *Building on 100 Years of Success: Proceedings of the 2006 International Thermal Spray Conference*, B.R. Marple, M.M. Hyland, Y.C. Lau, R.S. Lima, and J. Voyer, Ed., 15-18 May, 2006, Seattle, Washington, ASM International, 2006
30. S. Costil, H. Li, C. Coddet, V. Barnier, and R. Oltra, Role of Laser Surface Activation During Plasma Spray Coating of Metallic Materials, *18th International Conference on Surface Modification Technologies*, T.S. Sudarshan, M. Jeandin, and J.J. Stiglich, Ed., 15-17 November, 2004 (Dijon, France), ASM International, 2004, p 29-33
31. H. Li, S. Costil, V. Barnier, R. Oltra, O. Heintz, and C. Coddet, Surface Modifications Induced by Nanosecond Pulsed Nd:YAG Laser Irradiation of Metallic Substrates, *Surf. Coat. Technol.*, 2006, **201**, p 1383-1392
32. B. Arsenault, P. Gougeon, M. Verdier, and D.L. Duquesnay, Aluminum Protective Coatings—Fatigue and Bond Strength Properties with Respect to Surface Preparation Techniques: Laser Ablation, Shot Peening and Grit Blasting, *Can. Metall. Q.*, 2006, **45**(1), p 49-58
33. S. Costil, H. Liao, O. Chretien, A. Loredo, A. Gammoudi, M. Verdier, and C. Coddet, Influence of Laser Surface Cleaning Combined with Substrate Laser Preheating on Thermal Spray Coating Adhesion, *Lasers Eng.* , 2005, **15**(5-6), p 325-345
34. M. Verdier, G. Montavon, S. Costil, and C. Coddet, On the Adhesion Mechanisms of Thermal Spray Deposits Manufactured while Implementing the PROTAL® Process, *Proceedings of the International Thermal Spray Conference*, C.C. Berndt, K.A. Khor, and E.F. Laguscheider, Ed., 2001, p 553-560
35. S. Costil, M. Verdier, G. Montavon, and C. Coddet, Laser Surface Treatment for Subsequent Thermal Spray Deposition, *Lasers Eng.*, 2001, **11**(2), p 91-108
36. C. Coddet, G. Montavon, S. Ayrault-Costil, O. Freneaux, F. Rigolet, G. Barbezat, F. Folio, A. Diard, and P. Wazen, Surface Preparation and Thermal Spray in a Single Step: The PROTAL Process—Example of Application for an Aluminum-Base Substrate, *J. Therm. Spray Technol.*, 1999, **8**(2), p 235-242
37. Y. Ichikawa, K. Ogawa, M. Nivard, L. Berthe, M. Boustie, M. Ducos, S. Barradas, and M. Jeandin, Adhesion Study of Cold-Sprayed CoNiCrAlY-Mo Coating of Inconel 625 Using the LAser Shock Adhesion Test (LASAT), *Materials Science Forum*, Part 2 ed., 2007, p 1086-1091
38. S. Barradas, R. Molins, M. Jeandin, M. Arrigoni, M. Boustie, C. Bolis, L. Berthe, and M. Ducos, Application of Laser Shock Adhesion Testing to the Study of the Interlamellar Strength and Coating-Substrate Adhesion in Cold-Sprayed Copper Coating of Aluminum, *Surf. Coat. Technol.*, 2005, **197**, p 18-27
39. M. Boustie, E. Auroux, and J.P. Romain, Application of the Laser Spallation Technique to the Measurement of the Adhesion Strength of Tungsten Carbide Coatings on Superalloy Substrates, *Eur. Phys. J. Appl. Phys.*, 2000, **12**, p 47-53
40. C. Bolis, L. Berthe, M. Boustie, M. Arrigoni, S. Barradas, and M. Jeandin, Physical Approach to Adhesion Testing Using Laser-Driven Shock Waves, *J. Phys. D. Appl. Phys.*, 2007, **40**, p 3155-3163
41. Y. Liang, X. Bi, and J. Wang, Numerical Simulation of Laser-Induced Thin Film Delamination, *Thin Solid Films*, 2008, **516**, p 971-981
42. M. Boustie, J.P. Cuq-Lelandais, C. Bolis, L. Berthe, S. Barradas, M. Arrigoni, T. de Resseguier, and M. Jeandin, Study of Damage Phenomena Induced by Edge Effects into Materials Under Laser Driven Shocks, *J. Phys. D. Appl. Phys.*, 2007, **40**, p 7103-7108
43. E. Irissou, J.-G. Legoux, C. Moreau, and N. Ryabinin, How Cold is Cold Spray? An Experimental Study of the Heat Transfer to the Substrate in Cold Gas Dynamic Spraying, *Thermal Spray 2008: Thermal Spray Crossing Borders*, on CD-ROM, E. Lugscheider, Ed., June 2-4, 2008, Maastricht, The Netherlands, DVS Deutscher Verband für Schweißen, 2008, p 625-631
44. ImageJ Version 1.38x, Wayne Rasband, National Institute of Health, USA. http://rsb.info.nih.gov/ij/
45. G.R. Johnson, Material Characterisation for Warhead Computations, *Prog. Astronaut. Aeronaut.*, 1993, **155**, p 165-197
46. G.R. Johnson and W.H. Cook, A Constitutive Model and Data for Metals Subjected to Large Strains, High Strain Rates and High Temperatures, *Proceedings of the 7th Symposium on Ballistics*, The Hague, The Netherlands, 1983, p 541-547
47. W. Dabboussi and J.A. Nemes, Modeling of Ductile Fracture Using the Dynamic Punch Test, *Int. J. Mech. Sci.*, 2005, **47**(8), p 1282-1299
48. S. Costil, H. Li, and C. Coddet, New Developments in the PROTAL® Process, *Thermal Spray 2004: Thermal Spray Solutions—Advances in Technology and Application*, on CD-ROM,

10-12 May, 2004 (Osaka, Japan), DVS Deutscher Verband für Schweißen
49. V.Y. Gertsman and Q.S.M. Kwok, TEM Investigation of Nanophase Aluminum Powder, *Microsc. Microanal.*, 2005, **11**(5), p 410-420
50. P. Li, S. Xi, and J. Zhou, Phase Transformation and Gas-Solid Reaction of Al_2O_3 During High-Energy Ball Milling in N_2 Atmosphere, *Ceram. Int.*, 2009, **35**(1), p 247-251
51. E. Gaffet, D. Michel, L. Mazerolles, and P. Berthet, Effects of High Energy Ball Milling on Ceramic Oxides, *Mater. Sci. Forum*, 1997, **235-238**, p 103-108
52. Y. Xiong, K. Kang, G. Bae, S. Yoon, and C. Lee, Dynamic Amorphization and Recrystallization of Metals in Kinetic Spray Process, *Appl. Phys. Lett.*, 2008, **92**(19), p 19401-19404
53. C. Borchers, F. Gartner, T. Stoltenhoff, H. Assadi, and H. Kreye, Microstructural and Macroscopic Properties of Cold Sprayed Copper Coatings, *J. Appl. Phys.*, 2003, **93**(12), p 10064-10070
54. C.-J. Li, H.-T. Wang, Q. Zhang, G.-J. Yang, W.-Y. Li, and H.L. Liao, Influence of Spray Materials and Their Surface Oxidation on the Critical Velocity in Cold Spraying, *J. Therm. Spray Technol.*, 2010, **19**(1-2), p 95-101
55. M. Grujicic, C.L. Zhao, W.S. DeRosset, and D. Helfritch, Adiabatic Shear Instability Based Mechanism for Particles/Substrate Bonding in the Cold Gas Dynamic Spray Process, *Mater. Des.*, 2004, **25**, p 681-688
56. M. Grujicic, J.R. Saylor, D.E. Beasley, W.S. DeRosset, and D. Helfritch, Computational Analysis of the Interfacial Bonding Between Feed-powder Particles and the Substrate in the Cold-Gas Dynamic-Spray Process, *Appl. Surf. Sci.*, 2003, **219**, p 211-227
57. T. Schmidt, F. Gärtner, and H. Kreye, High Strain Rate Deformation Phenomena in Explosive Powder Compaction and Cold Gas Spraying, *Thermal Spray 2003: Advancing the Science and Applying the Technology*, B. R. Marple and C. Moreau, Ed., 5-8 May, 2003, Orlando, FL, ASM International, 2003, p 9-18
58. K.I. Triantou, Ch.I. Sarafoglou, D.I. Pantelis, D.K. Christoulis, V. Guipont, M. Jeandin, A. Zaroulias, and M. Vardavoulias, A Microstructural Study of Cold Sprayed Cu Coatings on 2017 Al Alloy, *Thermal Spray 2008: Thermal Spray Crossing Borders*, E. Lugscheider, Ed., on CD-ROM, June 2-4, 2008, (Maastricht, The Netherlands), DVS Deutscher Verband für Schweißen, 2008, p 49-53
59. S. Shin, Y. Xiong, Y. Ji, H.J. Kim, and C. Lee, The Influence of Process Parameters on Deposition Characteristics of a Soft/Hard Composite Coating in Kinetic Spray Process, *Appl. Surf. Sci.*, 2008, **254**(8), p 2269-2275
60. T. Stoltenhoff, C. Borchers, F. Gartner, and H. Kreye, Microstructures and Key Properties of Cold-Sprayed and Thermally Sprayed Copper Coatings, *Surf. Coat. Technol.*, 2006, **200**(16-17), p 4947-4960
61. T.S. Price, P.H. Shipway, and D.G. McCartney, Effect of Cold Spray Deposition of a Titanium Coating on Fatigue Behavior of a Titanium Alloy, *J. Therm. Spray Technol.*, 2006, **15**, p 507-512
62. E. Irissou and B. Arsenault, Corrosion Study of Cold Sprayed Aluminum Coatings onto Al 7075 Alloy Substrates, *Thermal Spray 2007: Global Coating Solutions*, B.R. Marple et al., Ed., Beijing, China, May 14-16, 2007, ASM International, CD-ROM, p 549-554
63. M. Arrigoni, S. Barradas, M. Braccini, M. Dupeux, M. Jeandin, M. Boustie, C. Bolis, and L. Berthe, A Comparative Study of Three Adhesion Tests (EN 582, Similar to ASTM C633, LASAT, Bulge and Blister Test) Performed on Plasma Sprayed Copper Deposited on Aluminium 2017 Substrates, *J. Adhes. Sci. Technol.*, 2006, **20**(5), p 471-487
64. L. Tollier, R. Fabbro, and E. Bartnicki, Study of the Laser Driven Spallation Process by the Velocity Interferometer System for Any Reflector Interferometry Technique. I. Laser Shock Characterization, *J. Appl. Phys.*, 1998, **83**(3), p 1224-1230
65. L. Tollier, R. Fabbro, and E. Bartnicki, Study of the Laser Driven Spallation Process by the Velocity Interferometer System for Any Reflector Interferometry Technique. II. Experiment and Simulation of the Spallation Process, *J. Appl. Phys.*, 1998, **83**(3), p 1231-1237